

MUSE Reveals a Recent Merger in the Post-starburst Host Galaxy of the TDE ASASSN-14li

J. L. Prieto^{1,2}, T. Krühler³, J. P. Anderson⁴, L. Galbany^{2,5}, C. S. Kochanek^{6,7}, E. Aquino⁸, J. S. Brown⁶, Subo Dong⁹, F. Förster^{10,2}, T. W.-S. Holoién^{6,7,11}, H. Kuncarayakti^{2,5}, J. C. Maureira¹⁰, F. F. Rosales-Ortega¹², S. F. Sánchez⁸, B. J. Shappee^{13,14}, K. Z. Stanek^{6,7}

ABSTRACT

We present MUSE integral field spectroscopic observations of the host galaxy (PGC 043234) of one of the closest ($z = 0.0206$, $D \simeq 90$ Mpc) and best-studied tidal disruption events (TDE), ASASSN-14li. The MUSE integral field data reveal asymmetric and filamentary structures that extend up to $\gtrsim 10$ kpc from

¹Núcleo de Astronomía de la Facultad de Ingeniería, Universidad Diego Portales, Av. Ejército 441, Santiago, Chile

²Millennium Institute of Astrophysics, Santiago, Chile

³Max-Planck-Institut für Extraterrestrische Physik (MPE), Giessenbachstrasse 1, 85748 Garching, Germany

⁴European Southern Observatory, Alonso de Córdova 3107, Casilla 19001, Santiago, Chile

⁵Departamento de Astronomía, Universidad de Chile, Camino El Observatorio 1515, Las Condes, Santiago, Chile

⁶Department of Astronomy, Ohio State University, 140 West 18th Avenue, Columbus, OH 43210, USA

⁷Center for Cosmology and AstroParticle Physics, The Ohio State University, 191 W. Woodruff Ave., Columbus, OH 43210, USA

⁸Instituto de Astronomía, Universidad Nacional Autónoma de México, A.P. 70-264, 04510, D.F., México

⁹Kavli Institute for Astronomy and Astrophysics, Peking University, Yi He Yuan Road 5, Hai Dian District, Beijing 100871, China

¹⁰Centro de Modelamiento Matemático, Universidad de Chile, Av. Blanco Encalada 2120 Piso 7, Santiago, Chile

¹¹US Department of Energy Computational Science Graduate Fellow

¹²Instituto Nacional de Astrofísica, Óptica y Electrónica, Luis E. Erro 1, 72840 Tonantzintla, Puebla, México

¹³Carnegie Observatories, 813 Santa Barbara Street, Pasadena, CA 91101, USA

¹⁴Hubble and Carnegie-Princeton Fellow

the post-starburst host galaxy of ASASSN-14li. The structures are traced only through the strong nebular [O III] $\lambda 5007$, [N II] $\lambda 6584$, and $H\alpha$ emission lines. The total off nuclear [O III] $\lambda 5007$ luminosity is 4.7×10^{39} erg s $^{-1}$ and the ionized H mass is $\sim 10^4(500/n_e) M_\odot$. Based on the BPT diagram, the nebular emission can be driven by either AGN photoionization or shock excitation, with AGN photoionization favored given the narrow intrinsic line widths. The emission line ratios and spatial distribution strongly resemble ionization nebulae around fading AGNs such as IC 2497 (Hanny’s Voorwerp) and ionization “cones” around Seyfert 2 nuclei. The morphology of the emission line filaments strongly suggest that PGC 043234 is a recent merger, which likely triggered a strong starburst and AGN activity leading to the post-starburst spectral signatures and the extended nebular emission line features we see today. We briefly discuss the implications of these observations in the context of the strongly enhanced TDE rates observed in post-starburst galaxies and their connection to enhanced theoretical TDE rates produced by supermassive black-hole binaries.

Subject headings: accretion, accretion disks; black hole physics; galaxies: evolution; galaxies: active; galaxies: interactions

1. Introduction

When a star passes within the tidal radius of a supermassive black-hole (SMBH), the strong gravitational tidal forces can tear it apart, potentially producing a short-lived luminous flare known as a tidal disruption event (TDE; Rees 1988; Evans & Kochanek 1989; Strubbe & Quataert 2009). TDEs can be used to find SMBHs in the centers of galaxies, to study their mass function and its evolution in cosmic time, to study the properties of the disrupted star and the stellar debris, and to determine the SMBH mass and spin (see review by Komossa 2015, and references therein). The theoretical TDE rate in a galaxy with a single SMBH has been estimated to be $10^{-5} - 10^{-4}$ per year (e.g., Wang & Merritt 2004; Stone & Metzger 2016). However, if a galaxy or galaxy merger has created a SMBH binary, the TDE rate could increase by a few orders of magnitude (e.g., Chen et al. 2009, 2011). The TDE rate can also be higher in steep central stellar cusps (e.g., Magorrian & Tremaine 1999; Stone & van Velzen 2016).

In the last few years, $\gtrsim 50$ TDE candidates¹ have been identified at different wavelengths

¹See <https://tde.space>.

from γ -rays to optical (e.g., Esquej et al. 2007; Gezari et al. 2008; Arcavi et al. 2014; Holoien et al. 2014, 2016a,b). One of the most unexpected observational results from these discoveries was the finding by Arcavi et al. (2014) that a large fraction of TDEs have post-starburst hosts, galaxies with strong Balmer absorption lines (A-type stellar populations with ages $\sim 100 - 1000$ Myr) on top of a spectrum characteristic of an old (elliptical) stellar population with weak or no evidence for very recent star-formation (E+A galaxies; e.g., Zabludoff et al. 1996). In a follow-up study using SDSS galaxies and a larger TDE host sample, French et al. (2016) confirm this result and estimate that the observed TDE rate might be more than two orders of magnitude higher in galaxies with strong Balmer absorption features compared to normal galaxies. Given this puzzling observation and the theoretical expectation of enhanced TDE rates in galaxies with SMBH binaries, detailed studies of TDE host galaxies could provide important insights into the physical mechanism that produces this rate enhancement.

The All-Sky Automated Survey for SuperNovae (ASAS-SN; Shappee et al. 2014), a transient survey of the whole sky at optical wavelengths, has discovered three of the closest (90 – 220 Mpc) and best studied TDEs (ASASSN-14ae, Holoien et al. 2014; Brown et al. 2016a; ASASSN-14li, Holoien et al. 2016a; ASASSN-15oi, Holoien et al. 2016b), providing an excellent sample for detailed host galaxy studies. In particular, ASASSN-14li at $z = 0.0206$ ($D \simeq 90$ Mpc), discovered in November 2014, has been the best studied TDE to date at all wavelengths, including the optical/UV (Holoien et al. 2016a; Cenko et al. 2016; Brown et al. 2016b), radio (Alexander et al. 2016; van Velzen et al. 2016; Romero-Cañizales et al. 2016), X-rays (Holoien et al. 2016a; Miller et al. 2015), and mid-infrared (Jiang et al. 2016), as well as with theoretical modeling (Krolik et al. 2016). The archival, nuclear SDSS spectrum of the host galaxy of ASASSN-14li, PGC 043234 (VIII Zw 211; $M_{\star} \simeq 3 \times 10^9 M_{\odot}$), shows strong Balmer lines in absorption and no strong evidence for current star-formation (Holoien et al. 2016a). Indeed, the galaxy has the highest Lick $H\delta_A$ index in the TDE host sample studied by French et al. (2016), indicating a strong post-starburst stellar population in its nuclear region with an age of ~ 100 Myr.

In this letter, we present integral field spectroscopic observations of the host galaxy of ASASSN-14li and its surroundings obtained in early 2016. In Section §2 we discuss the observations and data reduction. In Section §3 we present the results and the analysis of the data. We discuss our results in Section §4. Throughout the paper, we assume a distance to ASASSN-14li of $D = 90.3$ Mpc corresponding to a linear scale of $0''.44/\text{kpc}$ (Holoien et al. 2016a).

2. Observations and Data Reduction

We observed the field of ASASSN-14li as part of the All-weather MUse Supernova Integral field Nearby Galaxies (AMUSING; Galbany et al. 2016) with the Multi Unit Spectroscopic Explorer (MUSE, Bacon et al. 2010) on ESO’s Very Large Telescope UT4 (Yepun). MUSE is a state-of-the-art integral field spectrograph with a field of view of 1 arcmin^2 and $0''.2$ spaxels. It covers the spectral range $4800\text{--}9300 \text{ \AA}$ with a resolving power of $R \simeq 1800\text{--}3000$. Our MUSE data were obtained on 2016-01-21 and consisted of four dithered exposures each with an integration time of 698 sec. The sky conditions were clear, and we measure a full-width-half-maximum for the stellar point-spread function of $1''.05$ at 5000 \AA and $0''.85$ at 9000 \AA , respectively.

We reduced the MUSE spectroscopy with version 1.2.1 of the pipeline provided by ESO (Weilbacher et al. 2014), which applies a bias, flat-field, illumination, field geometry correction and background subtraction. The wavelength solution was tied to arc lamp frames, refined using skylines in the science data and converted into the heliocentric reference frame. Observations of the spectrophotometric standard GD108, taken immediately after the science data, provided the flux calibration. The final product of this reduction process is a data cube with two celestial coordinates sampled at $0''.2$ and one wavelength dimension sampled at 1.25 \AA . We checked the astrometric zeropoint of the MUSE data using the SDSS DR12 (Alam et al. 2015) r and i -band images of the field. We found and corrected astrometric shifts of $1''.03$ in RA and $1''.33$ in Dec with respect to the SDSS images.

3. Results and Analysis

An initial inspection of the MUSE data immediately showed the presence of extended line emission around PGC 043234 that was not detected in the SDSS $ugriz$ images. The left panel of Figure 1 shows a full $1' \times 1'$ image of the continuum just to the blue of the nebular [O III] $\lambda 5007$ emission line (at $\sim 5100 \text{ \AA}$ in the observer’s frame) and the right panel shows an image including the nebular [O III] $\lambda 5007$ emission line and its underlying continuum (at $\sim 5110 \text{ \AA}$ in the observer’s frame). The extended source to the West of PGC 043234 is an edge-on background galaxy at $z = 0.1517$, measured using nebular emission lines from the galaxy, and the bright point-source to the South is a Galactic star. The extended features around PGC 043234 have strong [O III] $\lambda 5007$ in emission, and further analysis also reveals strong [N II] $\lambda 6584$ and $H\alpha$ emission at the same locations.

Figure 2 shows a false color image of the MUSE field around ASASSN-14li/PGC 043234. In blue is the continuum-subtracted [O III] $\lambda 5007$ emission line image, in green is the

continuum-subtracted [N II] $\lambda 6584$ emission line image, and in red is the *i*-band continuum flux image obtained from synthetic photometry of the MUSE data cube. We observe complex filamentary and asymmetric structures in the nebular emission around PGC 043234 that resemble a galaxy merger that is undetected in the continuum image. The emission extends to a projected distance of $\gtrsim 5$ kpc ($\gtrsim 11''$) from the nucleus of PGC 043234, with some isolated nebular emission regions at $\gtrsim 10$ kpc ($\gtrsim 23''$) from the nucleus. The “arm” structure to the North-West of PGC 043234 extends to ~ 5 kpc, with a resolved extended peak in nebular emission at ~ 1.2 kpc. There is also an extended region of strong nebular emission ~ 2 kpc to the East/North-East of PGC 043234 with multiple emission peaks.

The circles in Figure 2 define $1''$ radius apertures for regions with strong nebular emission that we will study in more detail. In order to extract the fluxes of the nebular emission lines free from the contamination of the stellar continuum, we modeled the stellar continuum in the spectrum of each region using stellar population synthesis models from STARLIGHT (Cid Fernandes et al. 2009) and following the prescriptions presented in Galbany et al. (2014). The $H\beta$ emission line is undetected in most of the regions and we estimate 3σ upper limits on the emission line fluxes following Shappee et al. (2013).

In Table 1 we present the measured properties of the regions defined in Figure 2, including the coordinates, projected distances (in kpc) and radial velocity differences (in km s^{-1} , measured from the [N II] $\lambda 6584$ line) with respect to the nucleus of PGC 043234, along with integrated line luminosities (corrected for Galactic extinction) for the strongest nebular emission lines ([O III] $\lambda 5007$, $H\beta$, $H\alpha$, and [N II] $\lambda 6584$). The nebular emission line luminosities of the nuclear region of PGC 043432 shown in Table 1 are also included after subtracting the best-fit STARLIGHT model for the absorption lines. The $H\alpha$ and $H\beta$ emission line luminosities for the nuclear region should be interpreted with caution given the very strong stellar absorption and the contribution from ASASSN-14li to the nuclear fluxes even at late epochs after its discovery (Brown et al. 2016b).

In Figure 3 we show the integrated spectra of the regions defined in Figure 2 with the highest [O III] $\lambda 5007$ line luminosities. In addition to $H\alpha$, $H\beta$, [O III], and [N II], the He II $\lambda 4686$ and [S II] $\lambda\lambda 6716, 6731$ nebular emission lines are clearly detected in the region NW1. From the detection of the [S II] doublet we can estimate the electron density of the nebula (Osterbrock & Ferland 2006). Using the `temden` task in IRAF, the measured [S II] $\lambda\lambda 6716, 6731$ flux ratio of 1.04, and an assumed electron temperature of $T_e = 10^4$ K, the estimated electron density for the region is $n_e \sim 500 \text{ cm}^{-3}$. This implies a recombination timescale of $t_{\text{rec}} \sim 200$ yr (Osterbrock & Ferland 2006). Note that the [S II] $\lambda 6731$ emission line lies at the wavelength of the telluric O_2 B-band absorption, making this estimate of the density prone to significant systematic uncertainties.

In Figure 4 we show the standard Baldwin-Phillips-Terlevich (BPT; Baldwin et al. 1981) emission line diagnostics diagram along with the $[\text{N II}]/\text{H}\alpha$ and $[\text{O III}]/\text{H}\beta$ flux ratios (in logarithmic scale) for all the nebular emission regions defined in Figure 2 and the nucleus of PGC 043234. The dashed and dotted lines in Figure 4 separate the main sources of photoionization of nebulae between star formation (starburst) and AGN activity as defined in Kewley et al. (2001, dashed line) and Kauffmann et al. (2003, dotted line). Shock excitation can also produce line ratios in the range of the BPT diagram between star-formation and AGN (e.g., Allen et al. 2008; Rich et al. 2011; Alatalo et al. 2016). The area inside the magenta region defined in Figure 4 contains values of the line ratios that can be explained by shock models (Alatalo et al. 2016).

All the $[\text{O III}] \lambda 5007$ and $[\text{N II}] \lambda 6584$ emitting line regions around PGC 043234, including its nucleus, are consistent with photoionization by an AGN, instead of current star-formation, and most of the values of the ratios are also consistent with shock models. Given the presence of late-time Balmer line contamination from TDE emission in the nucleus (Brown et al. 2016b), we also measured the line ratios using the archival SDSS spectrum of the host galaxy (obtained in 2007) using the same approach to subtracting the strong stellar absorption lines. The resulting SDSS emission line fluxes of the nuclear region are $\log([\text{N II}]/\text{H}\alpha) \simeq 0.19$ and $\log([\text{O III}]/\text{H}\beta) \simeq 0.38$, which still puts the nucleus in the AGN/shock region of the BPT diagram (see Figure 4).

4. Discussion

We have presented MUSE integral field spectroscopic observations of the nearby TDE ASASSN-14li host galaxy, PGC 043234, and its environment ($26 \text{ kpc} \times 26 \text{ kpc}$). These data reveal the presence of asymmetric and filamentary emission line structures that extend many kpc from the post-starburst host galaxy of ASASSN-14li (Figure 2). The extended ($\gtrsim 5 \text{ kpc}$) filamentary structures are traced only by the detection of strong nebular emission lines of $[\text{O III}] \lambda 5007$, $[\text{N II}] \lambda 6584$, and $\text{H}\alpha$, and are undetected in the continuum, as illustrated in Figure 2. The total off nuclear line luminosities are $4.7 \times 10^{39} \text{ erg s}^{-1}$, $1.8 \times 10^{39} \text{ erg s}^{-1}$, and $1.3 \times 10^{39} \text{ erg s}^{-1}$ for $[\text{O III}]$, $[\text{N II}]$, and $\text{H}\alpha$, respectively, which implies an off-nuclear ionized H mass of $M_{\text{ion}} \sim 10^4(500/n_e) M_{\odot}$ (Osterbrock & Ferland 2006).

The location of the main nebular emission line ratios for both the extended emission line regions and the nucleus of PGC 043234 in the BPT diagnostic diagram (Figure 4) are consistent with photoionization by an AGN or shock excitation, but not photoionization by current star-formation. We do not favor shock excitation models as an explanation for the line ratios because the nebular emission lines have a low average intrinsic velocity dispersion

of $\sim 40 \text{ km s}^{-1}$ and no broad wings. Fast shocks ($v \gtrsim 200 \text{ km s}^{-1}$) that can produce the observed line ratios seem incompatible with the line widths (Allen et al. 2008), while slow shocks ($v \lesssim 200 \text{ km s}^{-1}$) which might be compatible, but still broader, with the line widths do not reproduce the line ratios (Rich et al. 2011). Also, the He II $\lambda 4686$ to $H\beta$ line ratio of 0.6 in the NW1 region is higher than in most of the fast shock models (Allen et al. 2008). We therefore conclude that the emission lines are most likely photoionized by an AGN.

There are two lines of evidence that PGC 043234 was a weak AGN prior to the TDE. The first, discussed in Section §3, is that the stellar population-corrected SDSS archival spectrum from 2007 of the nuclear region has line ratios suggesting AGN activity. PGC 043234 is also associated with an unresolved FIRST (Becker et al. 1995) radio source with a luminosity of $L_{1.4\text{GHz}} \simeq 2.6 \times 10^{21} \text{ W Hz}^{-1}$ (Holoien et al. 2016a) or $\nu \times L_\nu \sim 4 \times 10^{37} \text{ erg s}^{-1}$ that is typical of low-luminosity AGN (e.g., Ho 1999). Although the radio luminosity could be produced by star formation, there is no evidence for current star formation in the host galaxy from either the SDSS/MUSE spectra or the overall spectral energy distribution (Holoien et al. 2016a). However, the upper limit on the soft X-ray luminosity of PGC 043234 from the ROSAT All-Sky Survey (Voges et al. 1999) of $L_X < 6 \times 10^{40} \text{ erg s}^{-1}$ (Holoien et al. 2016a; Miller et al. 2015), implies an ionizing luminosity which is too small to explain the extended emission line features. Using the $H\alpha$ luminosity of the brightest off-nuclear emission region (NW1), assuming case B recombination and following Keel et al. (2012), we estimate a minimum required ionizing luminosity from a central source of $L_{\text{ion}} \gtrsim 2 \times 10^{41} \text{ erg s}^{-1}$.

The production of strong emission lines can then be explained in two ways. First, the pre-TDE nucleus could be a Seyfert 2, with other lines of sight being exposed to much higher ionizing fluxes. Such ionization “cones” are observed around local Seyfert 2 AGN on similar physical scales (e.g., Wilson & Tsvetanov 1994; Keel et al. 2012). Second, the observed emission line structures also resemble Hanny’s Voorwerp, a large ionization nebula located 15–25 kpc from the galaxy IC 2497 (Lintott et al. 2009), and other ionization nebulae where the line emission is thought to be an echo of AGN activity in the recent past rather than a reflection of present day activity (e.g., Keel et al. 2012; Schweizer et al. 2013).

The [S II] doublet line ratio measured in the spectrum of the strongest [O III] $\lambda 5007$ emitting region (NW1) implies a recombination time that is short compared to the light travel time to the furthest emission line regions ($\sim 10^2$ years versus $\sim 10^4$ years), which suggests that the pre-TDE source would more likely be a Seyfert 2 rather than a Voorwerp. The short recombination timescale is also at odds with a “fossil nebula” interpretation (Binette & Robinson 1987). However, the possible systematics errors associated with the density estimate from the [S II] doublet line ratio, due to the dominant telluric absorption correction at that wavelength, makes this conclusion fairly uncertain. Also, the distribution of the

emission line regions around PGC 043234 do not clearly favor the geometry seen in Seyfert 2 ionization cones (e.g., Wilson & Tsvetanov 1994).

In either case, the overall morphology of the emission line features strongly indicates that PGC 043234 recently underwent a merger, leaving relatively dense gas on large scales with no associated stars. This is consistent with both recent AGN activity and the post-starburst spectrum of the galaxy, strongly supporting the galaxy-galaxy merger scenario proposed for E+A galaxies (Zabludoff et al. 1996; Goto 2005). The stellar continuum emission itself is quite smooth, suggesting that we are observing the merger at a relatively late time (e.g., Hopkins et al. 2008). In these late phases, we might expect a relatively compact SMBH binary in the nucleus of the host galaxy, which would then naturally produce a greatly enhanced TDE rate (e.g., Chen et al. 2009, 2011). This would be an exciting possibility for explaining the high TDE rates that appear to be associated with post-starburst galaxies (Arcavi et al. 2014; French et al. 2016), including the host of ASASSN-14li. Indeed, the detection of a radio source at ~ 2 pc from the nucleus of PGC 043234 in high resolution EVN observations could be explained by a companion AGN (Romero-Cañizales et al. 2016).

We thank Rick Pogge for valuable discussions. Support for JLP, LG, FF, HK are provided by FONDECYT through the grants 1151445, 3140566, 11130228, and 3140563, respectively, and by the Ministry of Economy, Development, and Tourism’s Millennium Science Initiative through grant IC120009, awarded to The Millennium Institute of Astrophysics, MAS. TK is supported through the S. Kovalevskaja Award to P. Schady. CSK and KZS are supported by NSF grants AST-1515876 and AST-1515927. SD is supported by Grant No. XDB09000000 from the Chinese Academy of Sciences and Project 11573003 supported by NSFC. TW-SH is supported by the DOE CSGF grant DE-FG02-97ER25308. BJS is supported by NASA through Hubble Fellowship grant HST-HF-51348.001. FF and JCM acknowledge support from Basal Project PFB03 and from Conicyt through the infrastructure Quimal project No. 140003. Based on observations made with ESO telescopes at Paranal Observatory under programme 096.D-0296(A).

REFERENCES

- Alam, S., Albareti, F. D., Allende Prieto, C., et al. 2015, *ApJS*, 219, 12
- Alatalo, K., Cales, S. L., Rich, J. A., et al. 2016, *ApJS*, 224, 38
- Alexander, K. D., Berger, E., Guillochon, J., Zauderer, B. A., & Williams, P. K. G. 2016, *ApJ*, 819, L25

- Allen, M. G., Groves, B. A., Dopita, M. A., Sutherland, R. S., & Kewley, L. J. 2008, *ApJS*, 178, 20-55
- Arcavi, I., Gal-Yam, A., Sullivan, M., et al. 2014, *ApJ*, 793, 38
- Bacon, R., Accardo, M., Adjali, L., et al. 2010, *Proc. SPIE*, 7735, 773508
- Baldwin, J. A., Phillips, M. M., & Terlevich, R. 1981, *PASP*, 93, 5
- Becker, R. H., White, R. L., & Helfand, D. J. 1995, *ApJ*, 450, 559
- Binette, L., & Robinson, A. 1987, *A&A*, 177, 11
- Brown, J. S., Shappee, B. J., Holoién, T. W.-S., et al. 2016a, *MNRAS*, 462, 3993
- Brown, J. S., et al. 2016b, *MNRAS*, submitted, arXiv:1609.04403
- Cenko, S. B., Cucchiara, A., Roth, N., et al. 2016, *ApJ*, 818, L32
- Chen, X., Madau, P., Sesana, A., & Liu, F. K. 2009, *ApJ*, 697, L149
- Chen, X., Sesana, A., Madau, P., & Liu, F. K. 2011, *ApJ*, 729, 13
- Cid Fernandes, R., Schoenell, W., Gomes, J. M., et al. 2009, *Revista Mexicana de Astronomía y Astrofísica Conference Series*, 35, 127
- Esquej, P., Saxton, R. D., Freyberg, M. J., et al. 2007, *A&A*, 462, L49
- Evans, C. R., & Kochanek, C. S. 1989, *ApJ*, 346, L13
- French, K. D., Arcavi, I., & Zabludoff, A. 2016, *ApJ*, 818, L21
- Galbany, L., Stanishev, V., Mourão, A. M., et al. 2014, *A&A*, 572, A38
- Galbany, L., Anderson, J. P., Rosales-Ortega, F. F., et al. 2016, *MNRAS*, 455, 4087
- Gezari, S., Basa, S., Martin, D. C., et al. 2008, *ApJ*, 676, 944-969
- Goto, T. 2005, *MNRAS*, 357, 937
- Ho, L. C. 1999, *ApJ*, 516, 672
- Holoién, T. W.-S., Prieto, J. L., Bersier, D., et al. 2014, *MNRAS*, 445, 3263
- Holoién, T. W.-S., Kochanek, C. S., Prieto, J. L., et al. 2016a, *MNRAS*, 455, 2918

- Holoien, T. W.-S., Kochanek, C. S., Prieto, J. L., et al. 2016b, MNRAS, accepted, arXiv:1602.01088
- Hopkins, P. F., Hernquist, L., Cox, T. J., & Kereš, D. 2008, ApJS, 175, 356-389
- Jiang, N., Dou, L., Wang, T., et al. 2016, arXiv:1605.04640
- Kauffmann, G., Heckman, T. M., Tremonti, C., et al. 2003, MNRAS, 346, 1055
- Keel, W. C., Chojnowski, S. D., Bennert, V. N., et al. 2012, MNRAS, 420, 878
- Kewley, L. J., Dopita, M. A., Sutherland, R. S., Heisler, C. A., & Trevena, J. 2001, ApJ, 556, 121
- Komossa, S. 2015, Journal of High Energy Astrophysics, 7, 148
- Krolik, J., Piran, T., Svirski, G., & Cheng, R. M. 2016, ApJ, 827, 127
- Magorrian, J., & Tremaine, S. 1999, MNRAS, 309, 447
- Miller, J. M., Kaastra, J. S., Miller, M. C., et al. 2015, Nature, 526, 542
- Lintott, C. J., Schawinski, K., Keel, W., et al. 2009, MNRAS, 399, 129
- Osterbrock, D. E., & Ferland, G. J. 2006, Astrophysics of gaseous nebulae and active galactic nuclei, 2nd. ed. by D.E. Osterbrock and G.J. Ferland. Sausalito, CA: University Science Books, 206
- Rees, M. J. 1988, Nature, 333, 523
- Rich, J. A., Kewley, L. J., & Dopita, M. A. 2011, ApJ, 734, 87
- Romero-Cañizales, C., Prieto, J. L., et al. 2016, submitted to ApJL, arXiv:1609.00010
- Schweizer, F., Seitzer, P., Kelson, D. D., Villanueva, E. V., & Walth, G. L. 2013, ApJ, 773, 148
- Shappee, B. J., Stanek, K. Z., Pogge, R. W., & Garnavich, P. M. 2013, ApJ, 762, L5
- Shappee, B. J., Prieto, J. L., Grupe, D., et al. 2014, ApJ, 788, 48
- Stone, N. C., & Metzger, B. D. 2016, MNRAS, 455, 859
- Stone, N. C., & van Velzen, S. 2016, ApJ, 825, L14
- Strubbe, L. E., & Quataert, E. 2009, MNRAS, 400, 2070

van Velzen, S., Anderson, G. E., Stone, N. C., et al. 2016, *Science*, 351, 62

Voges, W., Aschenbach, B., Boller, T., et al. 1999, *A&A*, 349, 389

Wang, J., & Merritt, D. 2004, *ApJ*, 600, 149

Weilbacher, P. M., Streicher, O., Urrutia, T., et al. 2014, *Astronomical Data Analysis Software and Systems XXIII*, 485, 451

Wilson, A. S., & Tsvetanov, Z. I. 1994, *AJ*, 107, 1227

Zabludoff, A. I., Zaritsky, D., Lin, H., et al. 1996, *ApJ*, 466, 104

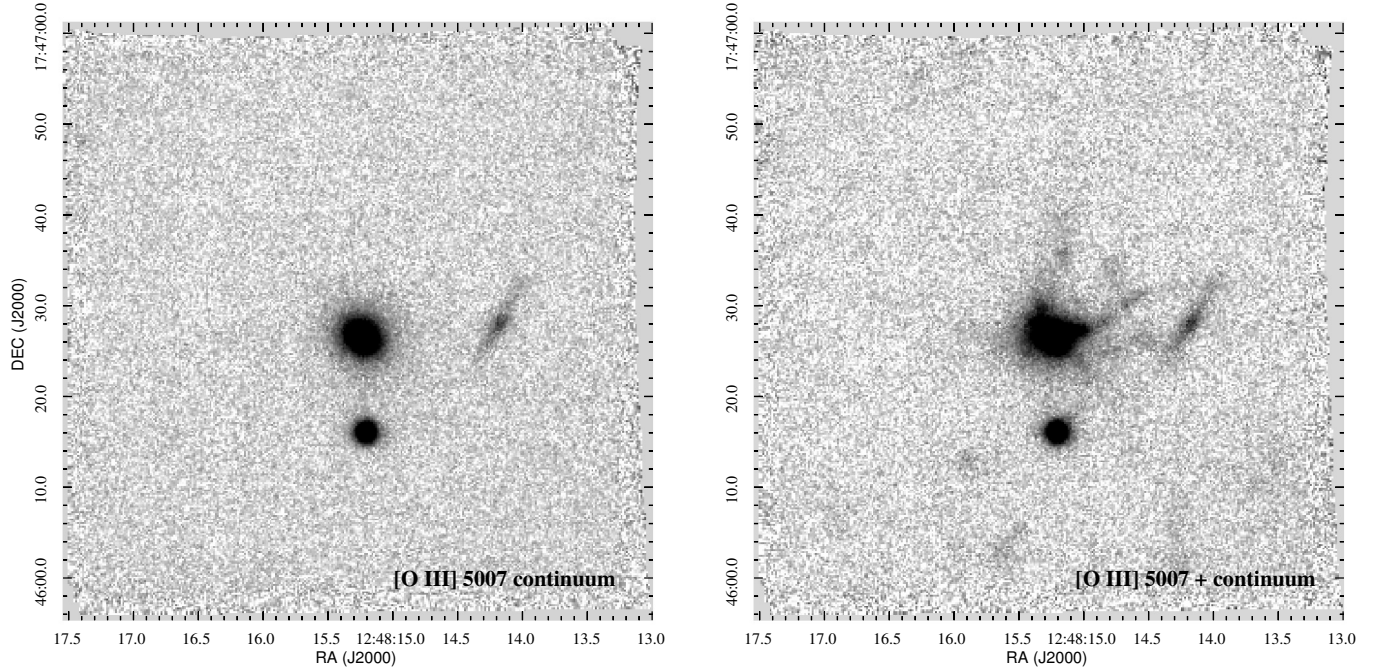


Fig. 1.— Grey scale images showing the full $1' \times 1'$ MUSE field centered on PGC 043234 (RA=12:48:15.24, DEC=+17:46:26.5), the host galaxy of the nearby TDE ASASSN-14li. The *left* panel shows an image of the continuum emission at 5100 \AA , just to the blue of the strong [O III] $\lambda 5007$ nebular line at the redshift of PGC 043234. The *right* panel shows an image at 5110 \AA which includes [O III] $\lambda 5007$ nebular line emission at the redshift of PGC 043234, that clearly reveals the presence of extended [O III] $\lambda 5007$ emission. The extended source to the west of PGC 043234 is a background edge-on galaxy at $z = 0.15$ (RA=12:48:14.18, DEC=+17:46:28.0) and the point source to the south of PGC 043234 is a foreground Galactic star (RA=12:48:15.21, DEC=+17:46:16.06).

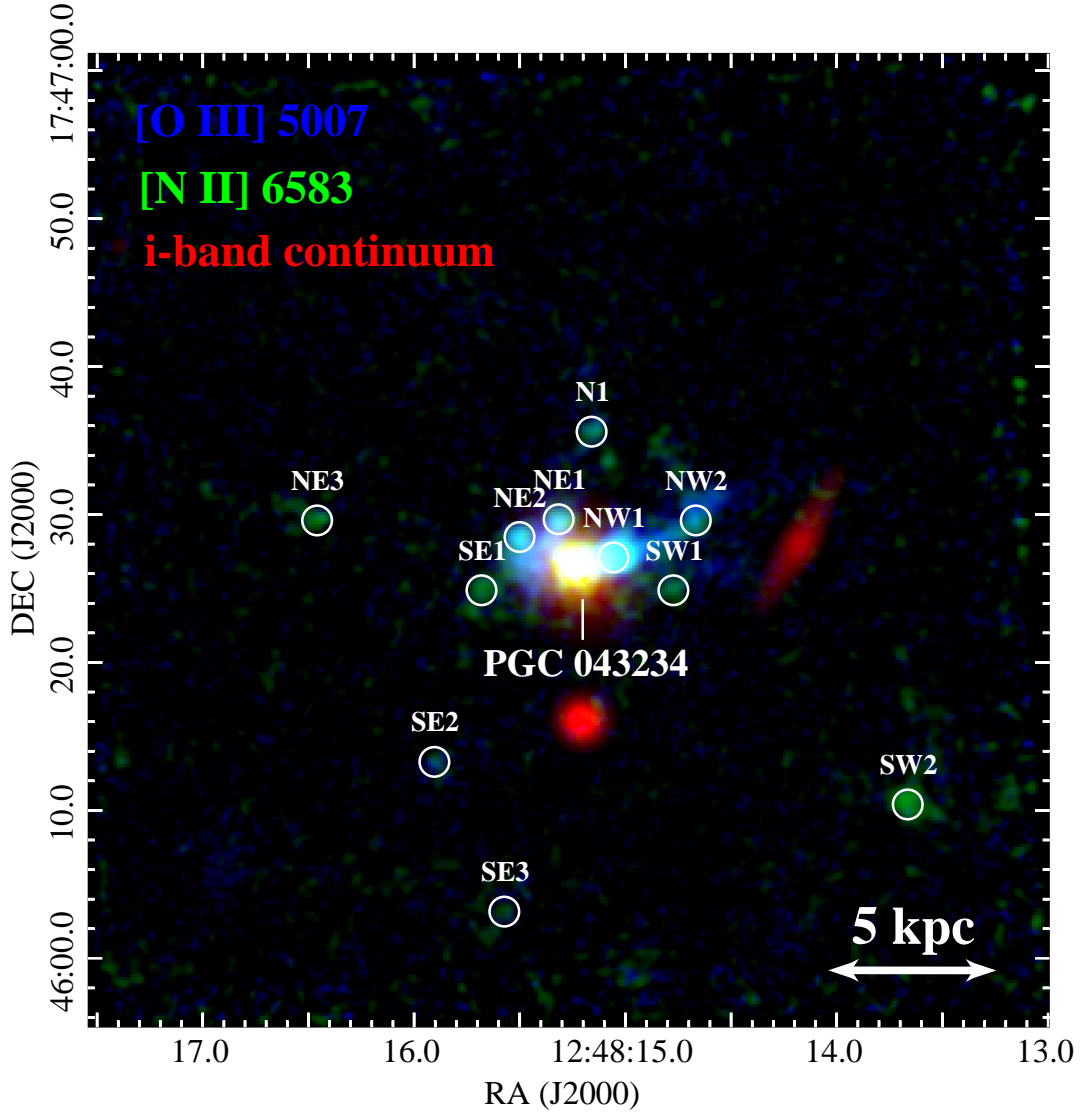


Fig. 2.— False color image showing the integrated, continuum-subtracted nebular emission of the [O III] $\lambda 5007$ (blue) and [N II] $\lambda 6584$ (green) lines at the redshift of PGC 043234 (center). The continuum emission (red) is traced by the SDSS *i*-band flux obtained from synthetic photometry. The [O III] $\lambda 5007$ and [N II] $\lambda 6584$ nebular line emission is distributed in the nucleus of PGC 043234 and around it, with large filamentary structures extending to ~ 12 kpc from the nucleus. The strongest [O III] $\lambda 5007$ emission is ~ 1.2 kpc to the North-West (region NW1) of the nucleus. The $1''$ radius circles with names are nebular emission regions defined for further analysis (see Table 1).

Table 1. Properties of the emission line regions defined in Figure 2.

| Location | RA (J2000.0) | DEC (J2000.0) | Δr (kpc) | Δv (km s ⁻¹) | L(H β) (10 ³⁷ erg s ⁻¹) | L([O III] λ 5007) (10 ³⁷ erg s ⁻¹) | L(H α) (10 ³⁷ erg s ⁻¹) | L([N II] λ 6584) (10 ³⁷ erg s ⁻¹) |
|----------|-----------------|------------------|---------------------|-------------------------------------|--|--|---|---|
| Nucleus | 12:48:15.24 | +17:46:26.5 | 0.0 | 0.0 | 23.7 | 80.7 | 57.3 | 39.4 |
| NW1 | 12:48:15.06 | +17:46:27.1 | 1.2 | +48 | 6.8 | 73.4 | 18.4 | 24.0 |
| NE1 | 12:48:15.32 | +17:46:29.7 | 1.5 | +12 | < 1.1 | 17.7 | 4.9 | 6.1 |
| NE2 | 12:48:15.50 | +17:46:28.5 | 1.8 | +88 | 3.0 | 17.2 | 4.6 | 6.4 |
| SE1 | 12:48:15.68 | +17:46:24.9 | 2.8 | -20 | < 0.9 | 3.8 | 1.1 | 2.6 |
| SW1 | 12:48:14.77 | +17:46:24.9 | 3.0 | -35 | < 0.8 | 4.2 | 1.4 | 2.2 |
| NW2 | 12:48:14.67 | +17:46:29.6 | 3.8 | +43 | < 1.0 | 10.2 | 2.9 | 3.9 |
| N1 | 12:48:15.16 | +17:46:35.6 | 4.0 | -9 | < 1.1 | 5.3 | 1.8 | 2.7 |
| SE2 | 12:48:15.90 | +17:46:13.3 | 7.1 | -20 | < 0.9 | 2.5 | 0.9 | 1.1 |
| NE3 | 12:48:16.46 | +17:46:29.6 | 7.8 | -4 | < 1.2 | 1.3 | 0.8 | 2.4 |
| SE3 | 12:48:15.57 | +17:46:03.2 | 10.4 | -17 | < 0.7 | 2.7 | 0.6 | 1.1 |
| SW2 | 12:48:13.66 | +17:46:10.4 | 12.1 | -20 | < 1.0 | 1.7 | 1.0 | 3.4 |

Note. — Δr and Δv are the projected distances (in kpc) and velocity shifts (relative to $v \simeq 6170$ km s⁻¹ for the central region of PGC 043234). The remaining columns are the H β , [O III] λ 5007, H α , and [N II] λ 6584 line luminosities of each region obtained after subtracting the stellar continuum using STARLIGHT models and correcting for Galactic extinction.

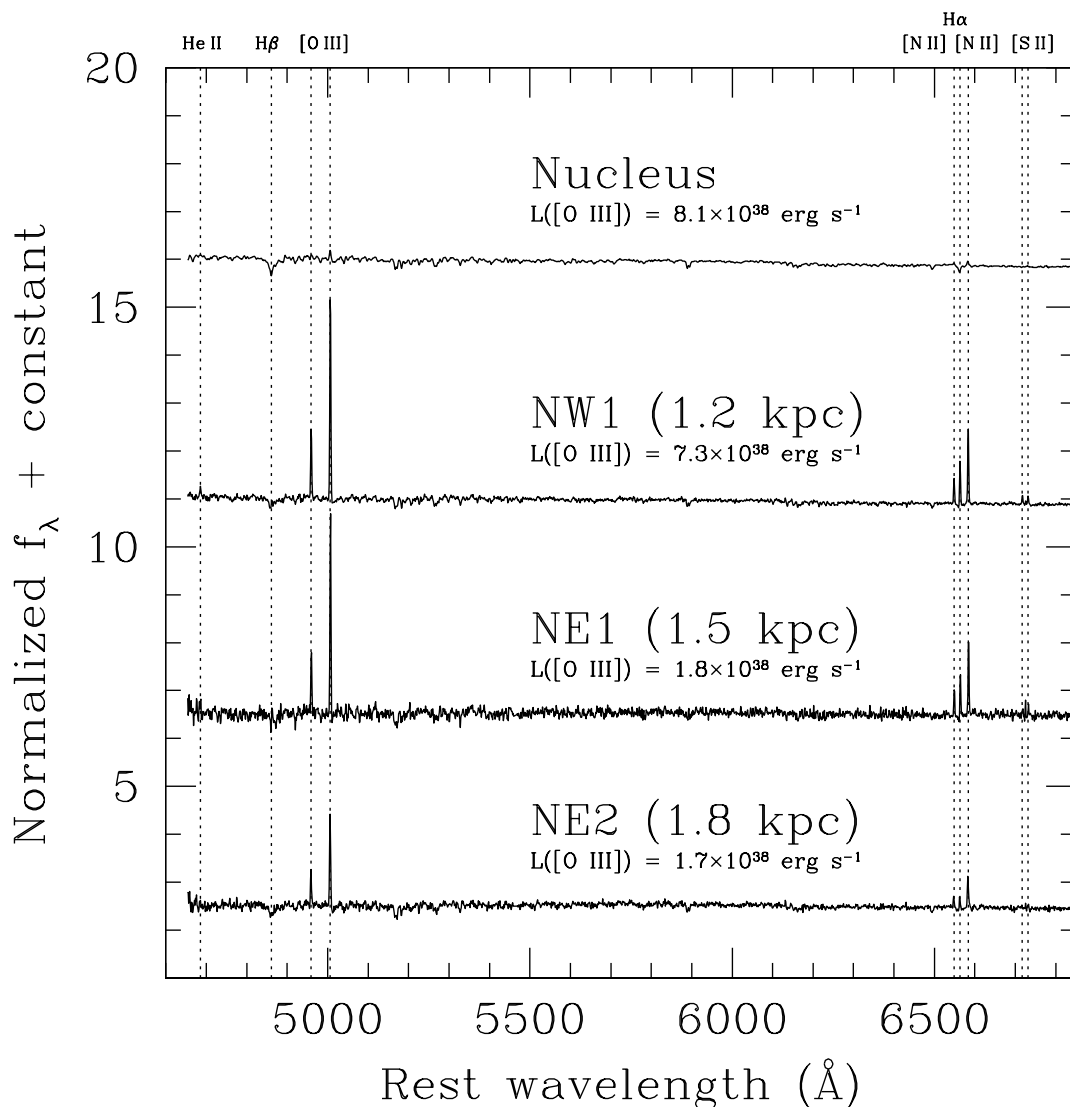


Fig. 3.— Integrated spectra ($1''$ aperture radius) of the strongest [O III] $\lambda 5007$ emission regions identified in Figure 2 and the nucleus of PGC 043234. Projected distances of each region from the nucleus are given in parenthesis. The main nebular emission lines in the spectra are [O III] $\lambda\lambda 4959, 5007$, [N II] $\lambda\lambda 6548, 6584$, and H α . Weaker nebular lines detected in NW1 are He II $\lambda 4686$, H β (also in absorption), and [S II] $\lambda\lambda 6716, 6731$. The dotted vertical lines show the rest wavelengths of the nebular emission lines. The spectra have been normalized by the local continuum at the [O III] $\lambda 5007$ line and shifted in flux for clarity.

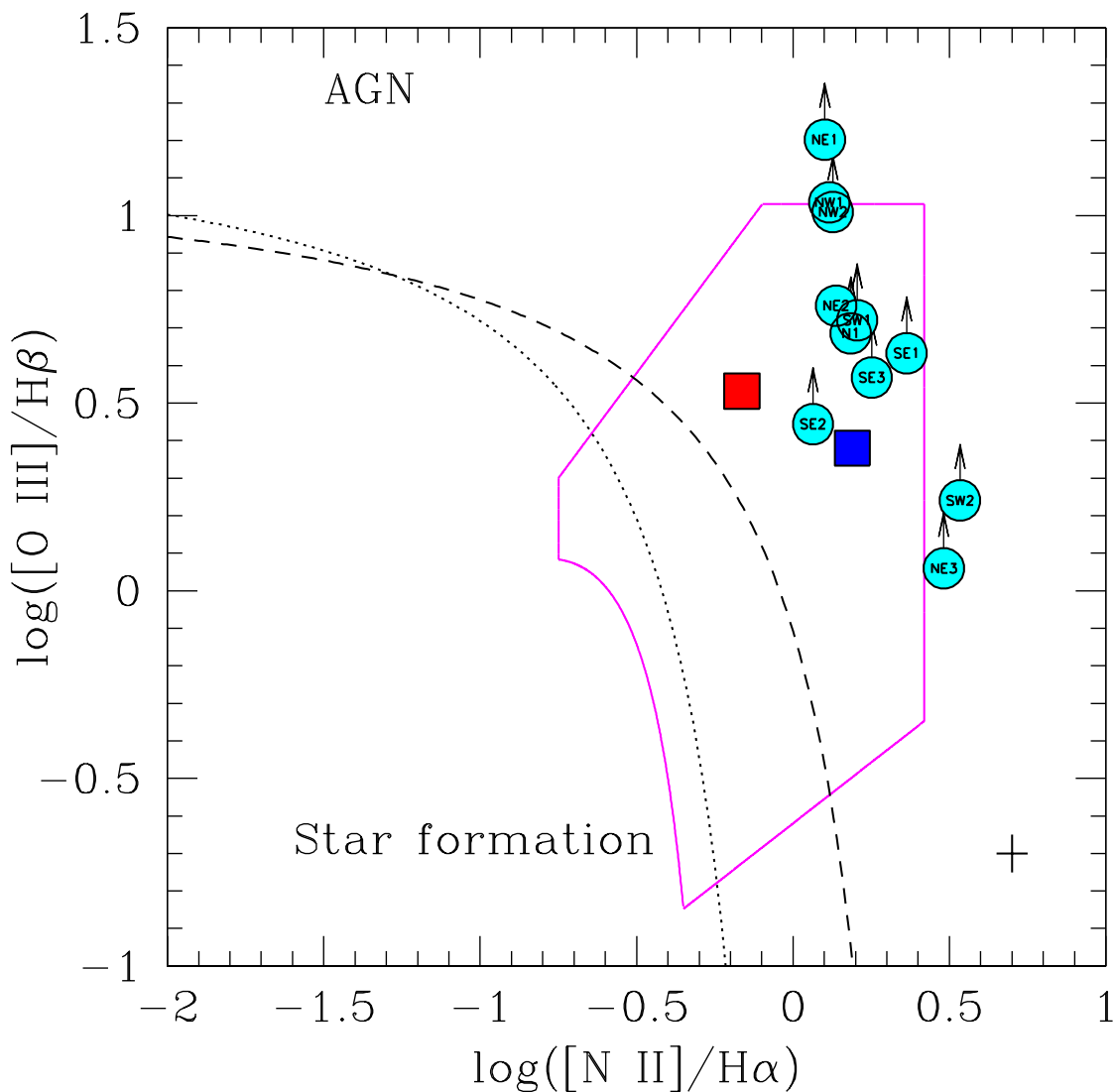


Fig. 4.— Nebular emission line ratio diagnostic (BPT; Baldwin et al. 1981) diagram for the nucleus of PGC 043234 (red filled square from MUSE and blue filled square from the SDSS 2007 archival spectrum) and the off-nuclear nebular line emission regions identified in Figure 2 (cyan filled circles). The dashed and dotted lines separate the dominant photoionization mechanisms between star-formation and AGN, as shown in Kewley et al. (2001) and Kauffmann et al. (2003), respectively. The line ratios inside the magenta region can also be explained by shocks (Alatalo et al. 2016). Average 1σ errors in the line ratios are shown in the lower right.